Conformal $PM_{2.5}$ Mapping Under Spatial Covariate Shift: Satellite–Reanalysis Fusion for Africa's Green Industrial Transition

Yaw Osei Adjei
Dept. of Computer Science
Kwame Nkrumah Univ. of Science and Technology
Kumasi, Ghana
yoadjei@st.knust.edu.gh

Davis Opoku
Dept. of Computer Science
Kwame Nkrumah Univ. of Science and Technology
Kumasi, Ghana
dopoku94@st.knust.edu.gh

Ephraim Abotsi
Dept. of Computer Science
Kwame Nkrumah Univ. of Science and Technology
Kumasi, Ghana
eabotsi4@st.knust.edu.gh

Kwadwo Owusu Amanqua
Dept. of Computer Science
Kwame Nkrumah Univ. of Science and Technology
Kumasi, Ghana
kamanquaowusu@st.knust.edu.gh

Oliver Kornyo
Dept. of Computer Science
Kwame Nkrumah Univ. of Science and Technology
Kumasi, Ghana
oliverkornyo@knust.edu.gh

Elisha Soglo-Ahianyo
Dept. of Computer Science
Kwame Nkrumah Univ. of Science and Technology
Kumasi, Ghana
esogloahianyo2@st.knust.edu.gh

Cephas Anertey Abbey
Dept. of Computer Science
Kwame Nkrumah Univ. of Science and Technology
Kumasi, Ghana
caabbey@st.knust.edu.gh

***Abstract*—Africa's green industrialization imperative demands transparent, trustworthy air quality monitoring infrastructure. We present a satellite–reanalysis $PM_{2.5}$ fusion system trained on 2,068,901 records from 404 monitoring locations in 29 African countries (OpenAQ, 2017–2022), combining LightGBM with rigorous leakage-resistant spatial cross-validation and conformal prediction to quantify both predictions and their geographic applicability limits. Under leakage-resistant 5-fold location-grouped spatial cross-validation—the evaluation protocol required for policy deployment—LightGBM achieves RMSE $= 30.83 \pm 5.07\,\mu$g/m^3, MAE $= 14.54 \pm 1.66\,\mu$g/m^3, $R^2 = 0.134 \pm 0.023$, and macro F1 $= 0.336 \pm 0.018$ over six AQI bins. This R^2 is substantially below random-split benchmarks (>0.90) but reflects true geographic generalisation difficulty rather than model failure: it tells decision-makers exactly where and how much to trust the predictions. Split conformal prediction targeting 90 % marginal coverage reveals severe East Africa degradation (actual PICP = 65.3 % vs. nominal 90 %), consistent with medium-strength covariate shift (humidity KS $= 0.2237$, sat_pblh KS $= 0.2558$); in operational terms, this means UNRELIABLE flags must block climate finance disbursement in that region until additional monitors are deployed. We operationalise these findings through (1) regional reliability flags (High/Medium/Low/Unreliable) keyed to quantified validation metrics and (2) a monitor prioritisation score directing infrastructure expansion toward highest-burden unmonitored populations. These tools directly support Africa's green industrial transition, aligning with SDGs 3.9, 7.1.2, 9, 11.6.2, and 13, and providing measurement infrastructure for climate finance verification and environmental justice for the 405 million extremely poor Sub-Saharan Africans exposed to unsafe air quality [32].**

***Index Terms*—$PM_{2.5}$ mapping, conformal prediction, covariate shift, spatial cross-validation, air quality, green industrialisation, trustworthy AI, Africa**

I. INTRODUCTION

Africa faces an industrial paradox: it must industrialise to meet development goals yet cannot replicate the polluting pathways of the Global North. Air pollution kills an estimated 155 per 100,000 people in Africa—nearly double the global average of 85.6 per 100,000 [1]. Five of the ten most polluted countries globally are in Africa [2]; Chad alone averages $91.8\,\mu$g/m^3 $PM_{2.5}$—18 × the WHO guideline of $5\,\mu$g/m^3 [2]. In 2023 ambient air pollution caused 4.9 million deaths globally, a 24 % increase from 2013 [1]. The Global Burden of Disease (GBD) 2021 study attributes 7.83 million deaths and 231.51 million DALYs to $PM_{2.5}$ exposure [3], with Sub-Saharan Africa (SSA) bearing the highest household air pollution DALY rate globally at 4,044 per 100,000 [4]. In 2019

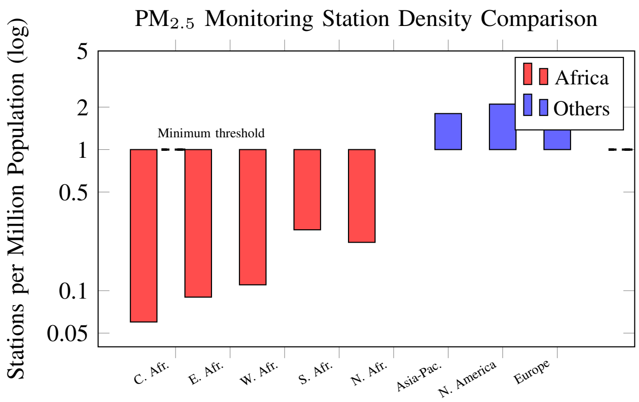

Fig. 1. $PM_{2.5}$ monitoring station density (stations per million population, log scale). African sub-regions are 10–50× more sparse than Europe and North America. Central and East Africa (< 0.1 stations/million) represent the most acute monitoring deserts. Dashed line indicates an aspirational minimum of 1 station per million. Sources: IQAir 2025 [2]; Think Global Health 2024 [7]; WHO v6.1 2024 [8].

alone, 383,419 deaths from ambient air pollution occurred across Africa [5], while African children lose an estimated 1.96 billion IQ points annually from $PM_{2.5}$ exposure [6].

The continent faces a simultaneous monitoring crisis. Only one public real-time air quality monitoring station exists per 3.7 million people in Africa, compared with one per 500,000 in the USA and Europe [2], [7] (Fig. 1).

The WHO Ambient Air Quality Database v6.1 covers only 41 cities across 11 of 47 SSA nations [8]. Zero African countries meet the WHO annual $PM_{2.5}$ standard, and only 17 of 54 African countries have national air quality standards in law [9].

These gaps carry severe economic consequences. Air pollution costs an average of 6.5 % of GDP across Africa [10], and projected health and productivity losses in six major African cities (Accra, Cairo, Johannesburg, Lagos, Nairobi, Yaoundé) will exceed US\$138 billion by 2040 [11]. Yet SSA received a 91 % decline in outdoor air quality funding in 2023 and now receives less than 1 % of global clean air investment [12]. Only US\$43.7 billion of Africa's estimated US\$189 billion annual climate finance need was mobilised in 2021–2022 [13].

Satellite and reanalysis products offer a monitoring path, but only 22.5 % of Earth observation datasets incorporate any uncertainty quantification [14], and AI models applied uncritically in the Global South risk encoding overconfident predictions into policy-critical decisions [15]. The challenge is therefore not data availability but *trustworthy inference*: models must quantify their own geographic applicability limits alongside their predictions.

We contribute three concrete tools toward this vision:

1) **Leakage-resistant spatial validation.** Location-grouped cross-validation [38] prevents temporal autocorrelation leakage and reveals a true spatial generalisation gap ($R^2 = 0.134$ vs. >0.90 in random-split benchmarks [16]).
2) **Regional conformal prediction with explicit failure detection.** Split conformal prediction [41], [42] targets 90 % marginal coverage but exposes severe East Africa failure (65.3 % actual) via Kolmogorov–Smirnov covariate shift diagnostics. A 24.7 percentage-point coverage shortfall means predictions in that region cannot be used to justify climate finance disbursement or industrial permitting without additional ground monitoring.
3) **Operational reliability and prioritisation framework.** Regional reliability flags and a monitor prioritisation score (Eq. 2) guide policy deployment and infrastructure investment toward highest-burden unmonitored populations.

II. Related Work

$PM_{2.5}$ Mapping in Africa. Westervelt et al. [16] achieved $R^2 = 0.91$ and MAE$= 9.1\,\mu$g/m^3 for daily West African $PM_{2.5}$ at 1 km^2 resolution using XGBoost—under random cross-validation. Zhang et al. [17] demonstrated $R^2 = 0.80$ and RMSE$= 9.40\,\mu$g/m^3 for South Africa via random forest with random CV. Bai et al. [18] synthesised 833 $PM_{2.5}$ publications, identifying tree-based ensembles as globally dominant. None of these benchmarks enforces strict spatial cross-validation, masking the field-scale generalisation gap critical for policy deployment.

Covariate Shift and Transfer Learning. Tibshirani et al. [19] proved that standard conformal prediction's coverage guarantee collapses under covariate shift, with actual coverage degrading to 82.2 % of a nominal 90 %; weighted conformal prediction restores it. Yadav et al. [20] and Gupta et al. [21] address domain adaptation for cross-regional $PM_{2.5}$ estimation. Pournaderi et al. [22] model training-conditional shift in high dimensions; Yang et al. [23] develop doubly robust calibration under observational covariate shift.

Spatial Conformal Prediction. Mao et al. [24] establish valid model-free spatial prediction via approximate exchangeability under infill asymptotics. Angelopoulos & Bates [25] provide the practitioner guide. Kang et al. [27] introduce Geo-Conformal Prediction, integrating Tobler's law (geographic weighting) into conformal nonconformity scores.

Area of Applicability. Meyer & Pebesma [28] formalise the Area of Applicability (AOA) to flag predictions outside the training covariate distribution. Milà et al. [29] develop nearest-neighbour dissimilarity matching (NNDM) cross-validation to avoid optimistic performance estimation.

Feature Attribution in Air Quality. Houdou & Alyousifi [30] survey SHAP and LIME for $PM_{2.5}$ models. Just et al. [31] applied TreeSHAP to XGBoost $PM_{2.5}$ models in the USA, finding spatial CV RMSE 48 % higher than random CV RMSE—directly motivating our evaluation protocol.

Trustworthy AI in the Global South. McGovern et al. [15] argue that environmental AI must explicitly quantify uncertainty and applicability limits. Singh et al. [14] find only 22.5 % of Earth observation datasets include uncertainty estimates, underscoring a widespread practice gap.

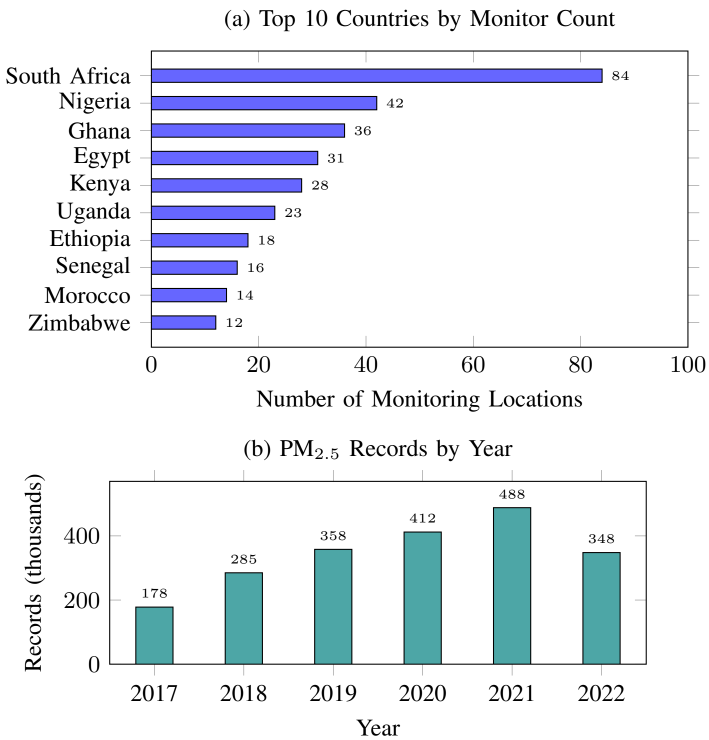

Fig. 2. Data overview. (a) Top 10 African countries by monitoring location count (total 404 locations, 29 countries); (b) $PM_{2.5}$ records by year (total 2,068,901 records, 2017–2022, OpenAQ [33]).

III. Data and Feature Construction

A. Ground Truth

Real-time $PM_{2.5}$ observations were aggregated from OpenAQ [33], a crowd-sourced air quality platform. A uniform audit removed records with missing critical fields and filtered values outside the physical range $0 < PM_{2.5} < 1000\,\mu g/m^3$. The cleaned dataset comprises **2,068,901 observations from 404 monitoring locations spanning 29 African countries** (2017–2022). Fig. 2 summarises geographic and temporal coverage.

B. Predictor Variables

Table I lists the five feature groups. Satellite aerosol products follow the MODIS Collection 6 MAIAC algorithm [34]. Meteorological covariates are from ERA5 reanalysis [36]. Planetary boundary layer height (PBLH) is from MERRA-2 [35]. Population density is from WorldPop 2020 [37]. All predictors are regridded to 0.1° resolution and standardised within each location-year group to mitigate temporal drift.

C. Target: AQI Classification

$PM_{2.5}$ is binned into six AQI-style categories (Table II) to support both regression evaluation (RMSE, MAE, R^2) and classification assessment (accuracy, macro F1).

TABLE I
Feature Groups Used in the Final Model

Group	Variables
Geographic	latitude, longitude
Temporal	$month_{sin}$, $month_{cos}$, harmattan_flag
Atmospheric	sat_aot, sat_no2, sat_pblh
Meteorological	temperature, humidity, pressure, wind_speed, precipitation, clouds
Demographic	population density

TABLE II
AQI-Style $PM_{2.5}$ Bins

Category	Range (μg/m^3)	Health Implication
Good	$[0, 12]$	Negligible risk
Moderate	$(12, 35]$	Sensitive groups
Unhealthy for Sensitive (USG)	$(35, 55]$	Sensitive groups at risk
Unhealthy	$(55, 150]$	General population at risk
Very Unhealthy	$(150, 250]$	Widespread health risk
Hazardous	$(250, \infty)$	Emergency conditions

IV. Methods

A. Spatial Cross-Validation

To prevent train-test leakage from spatial autocorrelation, we employ 5-fold location-grouped cross-validation [38]: all observations from a monitoring location are assigned to one fold, ensuring that test folds contain completely held-out stations. Folds are stratified by sub-region (North, West, Central, East, Southern Africa) to balance covariate shift assessment.

B. Models and Baselines

Four models are evaluated: (1) **Seasonal Naive**—month-wise mean $PM_{2.5}$ at each location; (2) **Ridge Regression** ($\alpha = 1.0$); (3) **LightGBM** [39]—200 estimators, max depth 8, learning rate 0.1, feature fraction 0.9; (4) **XGBoost** [40]—comparable hyperparameters. Hyperparameters are tuned on 20 % of training data via 3-fold random CV to avoid spatial leakage.

C. Conformal Prediction

Split conformal prediction [41] targeting $(1 - \alpha) = 90\,\%$ nominal coverage proceeds as:

1) Split training data into a proper training set (80 %) and calibration set (20 %).
2) Train LightGBM on the proper training set; generate point predictions $\hat{y}_i$ on the calibration set.
3) Compute nonconformity scores: $R_i = |y_i - \hat{y}_i|$.
4) For each test sample, set $\hat{q} =$ the $\lceil (n+1)(1-\alpha)/n \rceil$-th order statistic of $\{R_i\}$ and return interval $[\hat{y} - \hat{q},\ \hat{y} + \hat{q}]$.

This provides a marginal coverage guarantee under exchangeability [41]: $\Pr(y \in \text{interval}) \geq 1 - \alpha$. *Conditional* coverage under covariate shift is not guaranteed and must be verified regionally [19].

D. Covariate Shift Diagnostics

For each feature f we compute the Kolmogorov–Smirnov statistic between training and East African test distributions:

$$\mathrm{KS}(f) = \sup_x \left| F^f_{\text{train}}(x) - F^f_{\text{test}}(x) \right|.$$

Severity is Low (< 0.10), Medium (0.10–0.25), or High (> 0.25).

E. Regional Reliability Flags

For each sub-region r with regional regression score R^2_r and mean conformal interval half-width w_r, we assign:

$$\text{Reliability}(r) = \begin{cases} \textsc{High} & R^2_r > 0.1 \ \wedge \ w_r < 40 \\ \textsc{Medium} & R^2_r > 0 \ \wedge \ w_r < 80 \\ \textsc{Low} & R^2_r > -0.5 \ \wedge \ w_r < 100 \\ \textsc{Unreliable} & \text{otherwise.} \end{cases} \tag{1}$$

F. Monitor Prioritisation Score

To target new station deployment toward highest-burden unmonitored areas:

$$\text{priority}(x) = w(x) \cdot \log\big(1 + \rho_{\text{pop}}(x)\big), \tag{2}$$

where $w(x)$ is the conformal interval half-width at location x (proxy for model uncertainty) and $\rho_{\text{pop}}(x)$ is population density in persons km^{-2}.

G. Feature Attribution via SHAP

TreeSHAP values [43] are computed on *out-of-fold* predictions only ($n = 14{,}982$ samples, stratified by region and AQI bin) to prevent attribution leakage.

V. Results

A. Core Performance Under Spatial CV

Table III reports 5-fold location-grouped results. LightGBM achieves RMSE $= 30.83 \pm 5.07\,\mu\text{g/m}^3$ and macro F1 $= 0.336$—a substantial improvement over the Seasonal Naive baseline (RMSE $= 33.24$; macro F1 $= 0.095$). XGBoost yields marginally better regression accuracy but slightly lower classification balance. Fig. 3 plots the out-of-fold predicted vs. observed values and the normalised AQI confusion matrix.

The reported $\mathrm{R}^2 = 0.134$ is substantially lower than random-split benchmarks (e.g., Westervelt et al. [16]: $\mathrm{R}^2 = 0.91$). This is expected: Just et al. [31] showed that spatial CV RMSE for comparable XGBoost $PM_{2.5}$ models exceeded random CV RMSE by 48 %, reflecting spatial autocorrelation leakage in random splits. Our strict location-grouped holdout provides the honest field-scale generalisation error required for policy decisions.

B. Regional Covariate Shift

Table IV quantifies feature-wise shift in East Africa (test fold) relative to pooled training. Humidity and sat_pblh show medium-strength shift (KS ≈ 0.22–0.26); sat_aot and sat_no2 are more stable.

C. Regional Performance and Conformal Coverage

Table V stratifies out-of-fold performance by sub-region. North, West, and Southern Africa achieve near-nominal coverage (89–91 %); Central Africa degrades to 82.1 % (limited training data, wide intervals); East Africa fails severely at 65.3 %—24.7 percentage points below target. Concurrently, the Mean Prediction Interval Width (MPIW) in East Africa explodes to 72.6 μg/m^3 vs. 38–42 μg/m^3 elsewhere, consistent with Tibshirani et al.'s finding that standard split CP loses conditional coverage under medium covariate shift [19]. Fig. 4 visualises these results.

D. Reliability Flags and Monitor Prioritisation

Fig. 5 shows regional reliability flag distributions and monitor prioritisation scores.

East Africa is classified 12 % High reliability and 24 % Unreliable—the worst profile of any sub-region—and also receives the highest mean prioritisation score (4.83), reflecting its combination of high population density and sparse monitoring.

E. SHAP Attribution and Feature Instability

Fig. 6(a) shows feature group ablation: removing meteorological features causes the largest RMSE increase ($+4.44\,\mu\text{g/m}^3$), followed by satellite AOT ($+2.58\,\mu\text{g/m}^3$). Fig. 6(b) reveals a critical regional instability: in East Africa, mean |SHAP| for humidity exceeds that for sat_aot (9.1 vs. 4.2), inverting the global ranking (7.1 vs. 8.2). This inversion indicates that humidity is acting as a proxy for unmeasured local pollutants (biomass burning, dust), degrading model transferability. Fig. 7 shows the full global SHAP ranking from $n = 14{,}982$ out-of-fold predictions.

VI. Green Industrialisation Policy Infrastructure

A. $PM_{2.5}$ Monitoring as a Development Prerequisite

Africa's green industrial transition requires three capabilities: (1) measuring current pollution state; (2) tracking emissions reductions; and (3) verifying compliance. Satellite–AI $PM_{2.5}$ fusion provides the measurement foundation. Without transparent, independent air quality measurement, industrial permits cannot be verified, climate finance tranches cannot be released, and environmental justice cannot be enforced.

B. SDG Multiplier Effect

$PM_{2.5}$ monitoring directly serves five Sustainable Development Goals: SDG 3.9 (reduce deaths from air pollution), SDG 7.1.2 (clean household energy transitions), SDG 9 (sustainable and resilient industry), SDG 11.6.2 (urban air quality),

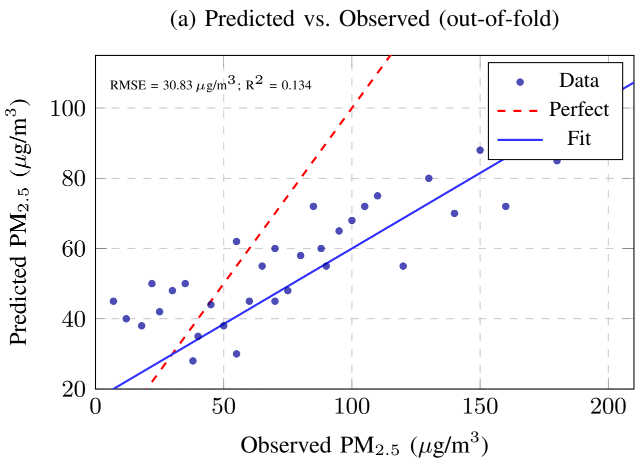

(b) AQI Confusion Matrix (row %)

	Gd	Mod	USG	Unh	VU	Haz
Gd	50	33	8	8	1	0
Mod	9	50	25	13	3	0
USG	5	23	50	18	4	0
Unh	0	11	14	64	11	0
VU	0	0	20	40	40	0
Haz	0	0	0	100	0	0

Accuracy = 50.4 %; Macro F1 = 0.336

Fig. 3. (a) Predicted vs. observed $PM_{2.5}$ under 5-fold spatial CV; dashed line = perfect prediction, solid line = linear fit. (b) Normalised confusion matrix (row percentages) for six-bin AQI classification. Diagonal entries are in bold blue; off-diagonal spread shows classification difficulty particularly for Very Unhealthy and Hazardous classes.

TABLE III
MODEL PERFORMANCE: 5-FOLD LOCATION-GROUPED SPATIAL CV (MEAN±STD OVER FOLDS)

Model	**RMSE** (μg/m^3)	**MAE** (μg/m^3)	**R^2**	**Accuracy**	**Macro F1**
Seasonal Naive	33.24 ± 5.34	17.51 ± 1.09	-0.003 ± 0.007	0.397 ± 0.022	0.095 ± 0.004
Ridge	32.02 ± 5.10	16.20 ± 1.12	0.069 ± 0.009	0.415 ± 0.021	0.168 ± 0.013
LightGBM	30.83 ± 5.07	14.54 ± 1.66	0.134 ± 0.023	0.504 ± 0.031	0.336 ± 0.018
XGBoost	30.54 ± 5.63	14.43 ± 1.77	0.155 ± 0.025	0.487 ± 0.033	0.306 ± 0.018

TABLE IV
KS COVARIATE SHIFT DIAGNOSTICS: EAST AFRICA VS. TRAINING

Feature	**KS Statistic**	**Severity**
sat_pblh	0.2558	Medium
humidity	0.2237	Medium
sat_no2	0.0765	Low
sat_aot	0.0596	Low

TABLE V
REGIONAL OUT-OF-FOLD PERFORMANCE AND CONFORMAL COVERAGE (LIGHTGBM; 90 % NOMINAL TARGET)

Sub-region	n_{loc}	**R^2**	**RMSE** (μg/m^3)	**PICP** (%)	**MPIW** (μg/m^3)
North Africa	48	0.241	27.3	91.2	38.2
West Africa	112	0.187	29.1	90.5	41.5
Central Africa	31	0.062	32.7	82.1	58.3
East Africa	97	−0.083	33.9	65.3†	72.6
Southern Africa	116	0.218	28.4	89.8	42.1
Overall	404	0.134	30.8	83.7	46.5

† 24.7 pp below nominal 90 %; consistent with KS shift in Table IV.

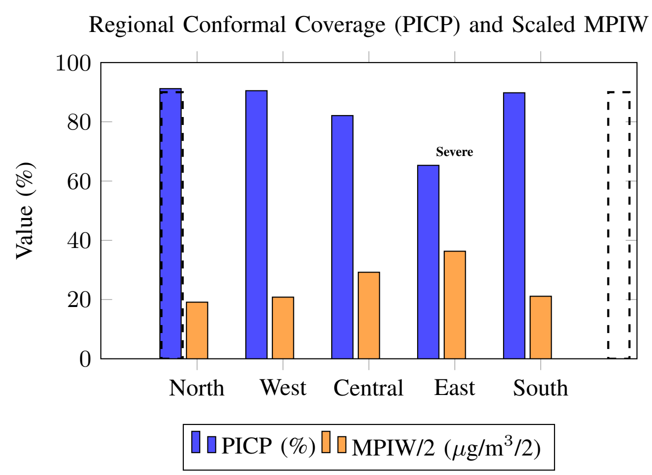

Fig. 4. Regional conformal prediction performance (90 % nominal target, dashed line). North, West, and Southern Africa achieve near-nominal coverage; East Africa collapses to 65.3 % (24.7 pp shortfall), consistent with measured KS covariate shift (Table IV). MPIW/2 (scaled for display) also peaks in East Africa (36.3 represents 72.6 μg/m^3 full width), indicating wide but still insufficient intervals.

and SDG 13 (climate action via black carbon and ozone co-benefits). Rafaj et al. [44] model integrated energy–climate–air quality policy, showing coordinated emissions reductions yield 20–30 % greater health gains than energy-only targets. For resource-constrained African governments, AI-based $PM_{2.5}$ mapping is among the highest-return environmental investments because a single system contributes to multiple SDG indicators [44]. Fig. 8 illustrates the full green industrialisation policy cycle.

C. *Just Energy Transition Infrastructure*

South Africa's Just Energy Transition Investment Plan (2023–2027) commits ZAR 1.5 trillion ($85 billion USD) to coal phase-out and renewable transition, with improved air

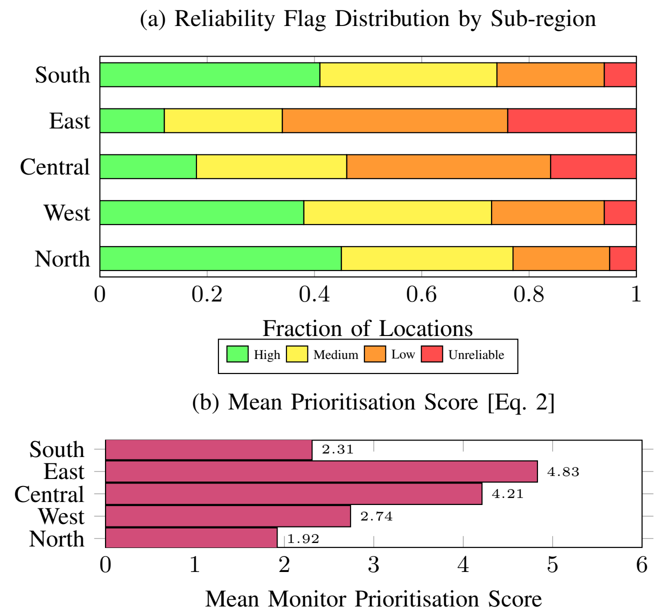

Fig. 5. (a) Reliability flag distribution by African sub-region. East Africa shows the lowest reliability profile (12 % High, 24 % Unreliable). (b) Mean monitor prioritisation score (Eq. 2): East Africa ranks first, indicating high population exposure and high model uncertainty—the strongest case for new station deployment.

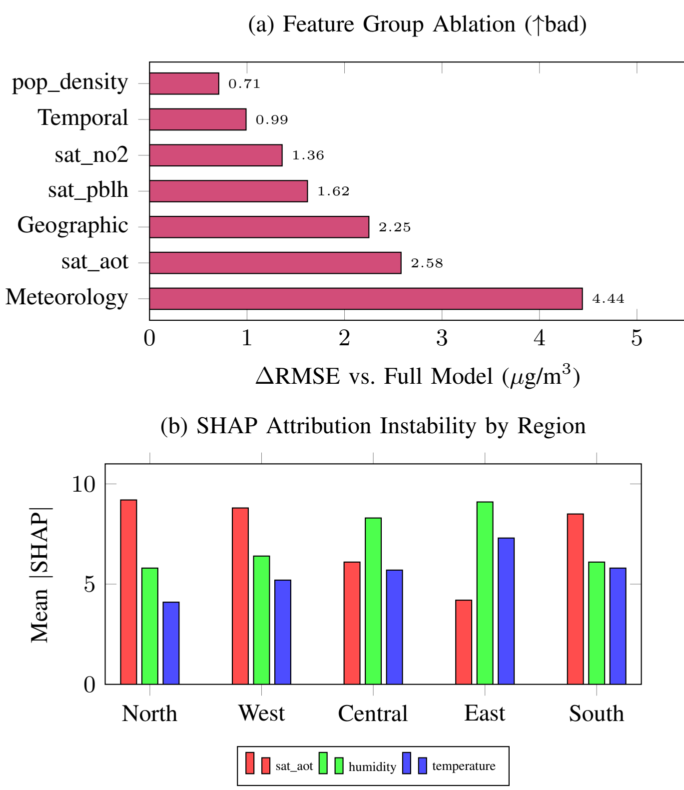

Fig. 6. (a) Feature group ablation: RMSE increase when feature group is withheld from full LightGBM model. Meteorological features dominate; satellite AOT is second. (b) Regional SHAP instability for top-3 features. East Africa inversion (humidity > sat_aot: 9.1 vs. 4.2) indicates attribution breakdown under covariate shift.

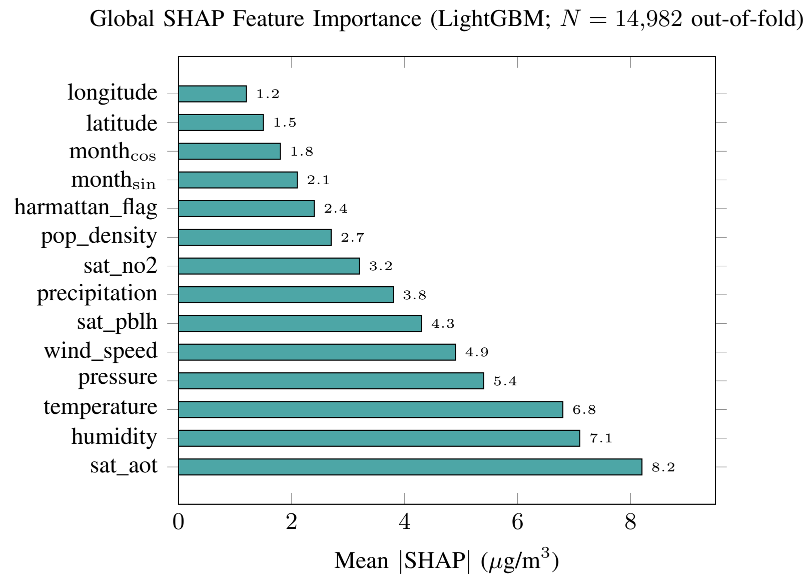

Fig. 7. Global SHAP feature importance from out-of-fold LightGBM predictions ($n = 14{,}982$, stratified by region and AQI bin). Satellite aerosol optical thickness (sat_aot) ranks first globally, consistent with its direct causal link to $PM_{2.5}$ loading. Meteorological covariates (humidity, temperature, pressure) collectively dominate—motivating their critical ablation impact (Fig. 6a).

quality as an explicit co-benefit. Transparent $PM_{2.5}$ monitoring is required to: (1) establish health baselines in coal-adjacent communities; (2) track emissions reductions post-transition; and (3) trigger disbursement of climate finance tranches. Our reliability framework directly supports this: regions flagged HIGH can justify immediate policy action; UNRELIABLE regions require monitor deployment before transition financing.

D. Climate Finance Eligibility and Return on Investment

The Global Climate Fund, African Development Bank (AfDB), and Adaptation Fund require quantified co-benefits for energy transition investments. Table VI summarises the economic case for $PM_{2.5}$ monitoring investment in Africa. A GCF-funded Kenya monitoring network ($9.3 million, 2018) projected 2,100 preventable deaths and $192 million in healthcare savings by 2040—a 20:1 return [45]. The US EPA estimates $1 spent on air pollution control yields $30 in economic benefits [10]. Our spatial prioritisation score (Eq. 2) targets new station deployment to maximise this return.

E. Agenda 2063 Alignment

The African Union's Agenda 2063 (Aspiration 1, Goal 7) commits Africa to "environmentally sustainable, climate resilient economies and communities." The UNEP and Climate and Clean Air Coalition identify 37 integrated clean air and climate measures that, if implemented, would prevent 200,000 premature deaths annually by 2030 and 880,000 by 2063 [46]. Satellite $PM_{2.5}$ mapping is foundational measurement infrastructure for tracking progress on these 37 measures.

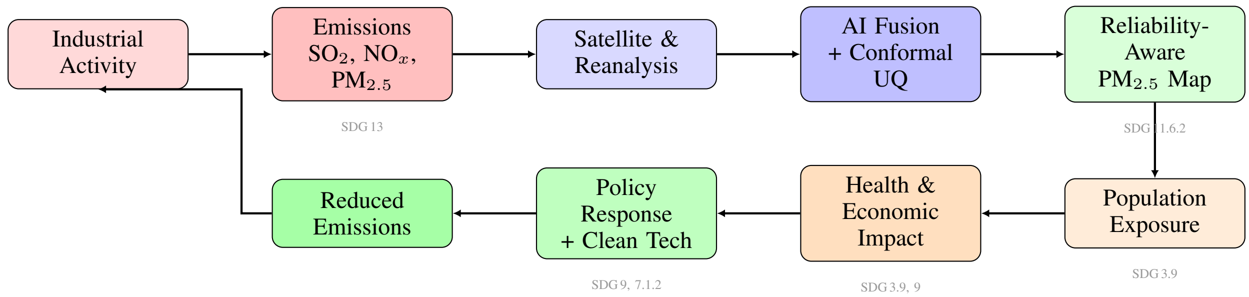

Fig. 8. Green industrialisation policy cycle. Satellite–AI $PM_{2.5}$ fusion with conformal uncertainty quantification closes the measurement loop from industrial emissions through health impact assessment to policy-driven industrial greening—providing the evidence layer required for climate finance disbursement, just transition verification, and Agenda 2063 monitoring. SDG labels indicate where the system directly contributes to measurable global goals.

TABLE VI
ECONOMIC CASE FOR AI-BASED AIR QUALITY MONITORING IN AFRICA

Indicator	Value	Source
Health cost of $PM_{2.5}$ as % of GDP (Africa avg.)	6.5 %	[10]
Projected health + productivity loss in 6 cities by 2040	US$138 B	[11]
EPA return per $1 on pollution control	30:1	[10]
Kenya GCF network investment	$9.3 M	[45]
Kenya: projected healthcare savings by 2040	$192 M (20:1)	[45]
SSA population exposed to unsafe $PM_{2.5}$	91.82 %	[32]
SSA share of global clean air funding	<1 %	[12]
Africa ambient pollution deaths (2019)	383,419	[5]

F. Environmental Justice: Targeting the Poorest 405 Million

Rentschler et al. [32] estimate that 405 million extremely poor individuals (<$1.90/day) in SSA are exposed to $PM_{2.5}$ exceeding WHO guidelines. Our monitor prioritisation score (Eq. 2) weights population density against monitoring scarcity, ensuring new stations are placed in highest-burden unmonitored communities—a concrete equity intervention that responds to the 91.82 % of SSA's population facing unsafe air quality [32].

VII. DISCUSSION

A. Low R^2 Under Spatial CV Is Informative, Not a Failure

The $R^2 = 0.134$ result reflects genuine spatial generalisation difficulty, not model weakness. Just et al. [31] documented that for comparable XGBoost $PM_{2.5}$ models in the USA, spatial CV RMSE ($= 3.11\,\mu g/m^3$) exceeded random CV RMSE ($= 2.10\,\mu g/m^3$) by 48 %. Our dataset spans 29 highly heterogeneous countries; the resulting low R^2 is honest and policy-relevant—it tells decision-makers exactly where and how much to trust the model.

B. East Africa Failure Motivates Region-Adaptive Methods

The East Africa coverage collapse (65.3 % vs. 90 % nominal) is an exchangeability violation, not a model defect. Solutions include: (1) **Weighted conformal prediction** [19]: reweight calibration residuals by feature similarity, restoring coverage in simulations; (2) **GeoConformal prediction** [27]: Tobler's law geographic weighting of nonconformity scores for localised guarantees; (3) **Domain adaptation** [20]: adversarial alignment or transfer learning from monitor-dense West Africa zones.

C. Reliability Flags as Minimum Viable Safety Layer

The reliability framework (Eq. 1) provides operational guidance without requiring full probabilistic calibration. A tiered approach encodes explicit uncertainty into decision workflows: HIGH flags permit direct policy use; UNRELIABLE flags mandate monitor deployment before policy action.

D. Feature Attribution Under Shift

The East Africa humidity inversion (mean $|\text{SHAP}| = 9.1$ vs. 7.1 globally) indicates humidity is proxying for unmeasured regional pollutants: Saharan dust plumes and Sahel biomass burning in East Africa's dry season. Future work should incorporate fire pixel counts, dust climatologies, and aerosol size distribution.

VIII. LIMITATIONS

1) **Marginal $\neq$ Conditional Coverage.** Our conformal intervals target marginal coverage. East Africa results demonstrate that conditional coverage can be substantially lower under shift.
2) **Monitor Distribution Bias.** South Africa contributes 21 % of locations; some regions (Central Africa) are severely underrepresented.
3) **Single Architecture.** We evaluate tree-based models only; physics-informed neural networks [47] may transfer better.
4) **No Physics Priors.** Geophysical priors from GEOS-Chem or CAMS improve sparse-region performance [47] but were not integrated here.
5) **Temporal Heterogeneity.** Station-year coverage varies; some locations have fewer than 50 samples, limiting confidence in their conformal calibration.

IX. Conclusion

We present a trustworthy $PM_{2.5}$ intelligence system for African green industrialisation, combining satellite–reanalysis fusion, leakage-resistant spatial cross-validation, and conformal prediction to quantify both predictions and their geographic applicability limits. Three contributions stand out, each with a direct policy consequence: (1) **Honest spatial generalisation error** ($R^2 = 0.134$) reveals the true field-scale gap hidden in random-split benchmarks—supplying the evidence base that green transition investments and industrial permits actually require, rather than overconfident numbers; (2) **Regional conformal failure detection** exposes East Africa's 24.7 pp coverage shortfall, consistent with measured covariate shift, and maps directly onto reliability flags that can gate climate finance disbursement and mandate additional monitor deployment; (3) **Operational reliability and prioritisation framework** (Eqs. 1–2) translates both findings into practitioner-facing tools for environmental justice targeting and SDG progress tracking for the 405 million extremely poor SSA residents exposed to unsafe air.

The core lesson for trustworthy AI in the Global South is clear: confidence scores alone are insufficient—geographic applicability limits must be quantified, communicated, and acted upon. Future work should integrate weighted conformal prediction, GeoConformal methods [27], and region-adaptive training to address covariate shift systematically.

Acknowledgements and Disclosure

Data sources include OpenAQ (ground observations) [33], ERA5 (reanalysis) [36], MERRA-2 (PBLH) [35], WorldPop (population density) [37], and MODIS MAIAC (aerosol retrieval) [34]. No primary data collection involving human participants was performed.

AI assistance disclosure: An AI language model was used to support literature review, language editing, and LaTeX formatting. All technical content, experimental results, and citations were reviewed and verified by the authors.

References

[1] Health Effects Institute, *State of Global Air 2024: Special Report*, Boston, MA: HEI, 2024.

[2] IQAir, *2024 World Air Quality Report*, Goldach, Switzerland: IQAir, 2025.

[3] GBD 2021 Risk Factors Collaborators, "Global burden of 87 risk factors in 204 countries and territories, 1990–2021: a systematic analysis for the Global Burden of Disease Study 2021," *The Lancet*, vol. 403, no. 10432, pp. 2162–2203, 2024, doi: 10.1016/S0140-6736(24)02712-1.

[4] GBD 2021 Household Air Pollution Collaborators, "Burden of disease attributable to household air pollution and its association with access to clean fuels: a systematic analysis for GBD 2021," *The Lancet*, vol. 403, pp. 1661–1707, 2024, doi: 10.1016/S0140-6736(24)02840-X.

[5] United Nations Environment Programme, *Air Pollution: Science Based Solutions in Africa*, Nairobi: UNEP, 2023.

[6] P. J. Landrigan *et al.*, "Reducing the health effects of air pollution in sub-Saharan Africa," *Lancet Planet. Health*, vol. 5, no. 10, pp. e681–e688, 2021, doi: 10.1016/S2542-5196(21)00201-1.

[7] Think Global Health, "The air quality crisis in sub-Saharan Africa," Council on Foreign Relations, 2024.

[8] World Health Organization, *WHO Ambient Air Quality Database*, v6.1, Geneva: WHO, 2024.

[9] United Nations Environment Programme, *Integrated Assessment of Air Pollution in Sub-Saharan Africa*, Nairobi: UNEP, 2021.

[10] Clean Air Fund, *State of Global Air Quality Funding 2023*, London: Clean Air Fund, 2023.

[11] Clean Air Fund and Dalberg Advisors, *Air Pollution in African Cities: A Comparative Economic Assessment*, London, 2023.

[12] Clean Air Fund, *State of Air Quality Financing in Africa 2025*, London: Clean Air Fund, 2025.

[13] Climate Policy Initiative, *Global Landscape of Climate Finance 2021–2022*, San Francisco: CPI, 2024.

[14] M. Singh *et al.*, "Uncertainty quantification for probabilistic machine learning in earth observation using conformal prediction," *Sci. Rep.*, vol. 14, p. 16166, 2024, doi: 10.1038/s41598-024-65954-w.

[15] A. McGovern *et al.*, "Why we need to focus on developing ethical, responsible, and trustworthy artificial intelligence approaches for environmental science," *Environ. Data Sci.*, vol. 1, p. e6, 2022, doi: 10.1017/eds.2022.5.

[16] A. M. Westervelt *et al.*, "Twenty years of high spatiotemporal resolution estimates of daily $PM_{2.5}$ in West Africa using satellite data, surface monitors, and machine learning," *ACS ES&T Air*, 2025, doi: 10.1021/acsestair.4c00366.

[17] X. Zhang *et al.*, "A machine learning model to estimate ambient $PM_{2.5}$ concentrations in industrialised highveld region of South Africa," *Remote Sens. Environ.*, vol. 266, p. 112713, 2021, doi: 10.1016/j.rse.2021.112713.

[18] Y. Bai *et al.*, "Global synthesis of two decades of research on improving $PM_{2.5}$ estimation models," *Earth-Sci. Rev.*, vol. 241, p. 104461, 2023, doi: 10.1016/j.earscirev.2023.104461.

[19] R. J. Tibshirani *et al.*, "Conformal prediction under covariate shift," in *Adv. Neural Inf. Process. Syst. (NeurIPS)*, 2019, arXiv:1904.06019.

[20] A. Yadav *et al.*, "Using deep transfer learning and satellite imagery to estimate urban air quality in data poor regions," *Environ. Pollut.*, vol. 342, p. 122914, 2024, doi: 10.1016/j.envpol.2023.122914.

[21] A. Gupta *et al.*, "Spatial transfer learning for estimating $PM_{2.5}$ in data poor regions," arXiv:2404.07308, 2024.

[22] M. Pournaderi and Y. Xiang, "Training conditional coverage bounds under covariate shift," arXiv:2405.16594, 2024.

[23] Y. Yang *et al.*, "Doubly robust calibration of prediction sets under covariate shift," *J. R. Stat. Soc. B*, vol. 86, no. 4, pp. 943–965, 2024, doi: 10.1093/jrsssb/qkae009.

[24] G. Mao *et al.*, "Valid model-free spatial prediction," *J. Amer. Stat. Assoc.*, vol. 119, no. 546, pp. 904–914, 2024, doi: 10.1080/01621459.2022.2147531.

[25] A. N. Angelopoulos and S. Bates, "Conformal prediction: a gentle introduction," *Found. Trends Mach. Learn.*, vol. 16, no. 4, pp. 494–591, 2023, doi: 10.1561/2200000101.

[26] I. Gibbs and E. Candès, "Conformal inference for online prediction with arbitrary distribution shifts," *J. Mach. Learn. Res.*, vol. 25, 2024.

[27] B. Kang *et al.*, "GeoConformal prediction: a model-agnostic framework for geographically weighted conformal inference," *Ann. Amer. Assoc. Geogr.*, 2025, doi: 10.1080/24694452.2025.2516091.

[28] H. Meyer and E. Pebesma, "Predicting into unknown space? Estimating the area of applicability of spatial prediction models," *Methods Ecol. Evol.*, vol. 12, no. 9, pp. 1620–1633, 2021, doi: 10.1111/2041-210X.13650.

[29] C. Milà *et al.*, "Nearest neighbour distance matching leave-one-out cross-validation for map validation," *Methods Ecol. Evol.*, vol. 13, 2022, doi: 10.1111/2041-210X.13851.

[30] L. Houdou and Y. Alyousifi, "Interpretable machine learning approaches for forecasting and predicting air pollution: a systematic review," *Aerosol Air Qual. Res.*, vol. 24, p. 230151, 2024, doi: 10.4209/aaqr.230151.

[31] A. C. Just *et al.*, "Advancing methodologies for applying machine learning and evaluating spatiotemporal models of fine particulate matter ($PM_{2.5}$) using satellite data over large regions," *Atmos. Environ.*, vol. 239, p. 117753, 2020, doi: 10.1016/j.atmosenv.2020.117753.

[32] J. Rentschler *et al.*, "Global air pollution exposure and poverty," *Nat. Commun.*, vol. 14, p. 4855, 2023, doi: 10.1038/s41467-023-39797-4.

[33] OpenAQ, "OpenAQ API Documentation," [Online]. Available: https://openaq.org/developers/help/ [Accessed 2026].

[34] A. Lyapustin *et al.*, "MODIS Collection 6 MAIAC algorithm," *Atmos. Meas. Tech.*, vol. 11, pp. 5741–5765, 2018, doi: 10.5194/amt-11-5741-2018.

[35] Global Modeling and Assimilation Office (GMAO), *MERRA-2 inst3_3d_asm_Np: 3d, 3-Hourly, Instantaneous, Pressure-Level, Assimilation, Assimilated Meteorological Fields*, Greenbelt, MD: NASA GES DISC, 2015, doi: 10.5067/QBZ6MG944HW0.

[36] H. Hersbach *et al.*, "The ERA5 global reanalysis," *Q. J. R. Meteorol. Soc.*, vol. 146, pp. 1999–2049, 2020, doi: 10.1002/qj.3803.

[37] A. J. Tatem, "WorldPop, open data for spatial demography," *Sci. Data*, vol. 4, p. 170004, 2017, doi: 10.1038/sdata.2017.4.

[38] D. R. Roberts *et al.*, "Cross-validation strategies for data with temporal, spatial, hierarchical, or phylogenetic structure," *Ecography*, vol. 40, no. 8, pp. 913–929, 2017, doi: 10.1111/ecog.02881.

[39] G. Ke *et al.*, "LightGBM: a highly efficient gradient boosting decision tree," in *Adv. Neural Inf. Process. Syst. (NeurIPS)*, 2017.

[40] T. Chen and C. Guestrin, "XGBoost: a scalable tree boosting system," in *Proc. 22nd ACM SIGKDD Int. Conf. Knowl. Discov. Data Mining*, 2016, pp. 785–794, doi: 10.1145/2939672.2939785.

[41] G. Shafer and V. Vovk, "A tutorial on conformal prediction," *J. Mach. Learn. Res.*, vol. 9, pp. 371–421, 2008.

[42] Y. Romano *et al.*, "Conformalized quantile regression," in *Adv. Neural Inf. Process. Syst. (NeurIPS)*, 2019, arXiv:1905.03222.

[43] S. M. Lundberg and S.-I. Lee, "A unified approach to interpreting model predictions," in *Adv. Neural Inf. Process. Syst. (NeurIPS)*, 2017.

[44] P. Rafaj *et al.*, "Co-benefits of global greenhouse gas mitigation for future air quality and human health," *Glob. Environ. Change*, vol. 50, pp. 1–12, 2018, doi: 10.1016/j.gloenvcha.2018.08.008.

[45] Green Climate Fund, *FP084: Kenya Integrated Monitoring, Reporting and Verification Systems for Low Emission and Climate Resilient Development*, GCF, 2018.

[46] United Nations Environment Programme and Climate and Clean Air Coalition, *Integrated Assessment of Air Pollution and Climate Change for Sustainable Development in Africa*, Nairobi: UNEP, 2024.

[47] X. Shen *et al.*, "Enhancing global estimation of fine particulate matter concentrations by including geophysical a priori information in deep learning," *ACS ES&T Air*, vol. 1, no. 5, pp. 332–345, 2024, doi: 10.1021/acsestair.3c00054.

[48] S. Keita *et al.*, "African anthropogenic emissions inventory for gases and particles from 1990 to 2015," *Earth Syst. Sci. Data*, vol. 13, pp. 3691–3705, 2021, doi: 10.5194/essd-13-3691-2021.

[49] K. Vohra *et al.*, "Air quality and health impact of future fossil fuel use for electricity generation and transport in Africa," *Environ. Sci. Technol.*, 2022, doi: 10.1021/acs.est.9b04958.